NASA Contractor Report 187188

Review of Nondiffracting Bessel Beams

Michael R. LaPointe
Sverdrup Technology, Inc.
Lewis Research Center Group
Brook Park, Ohio

August 1991

Prepared for
Lewis Research Center
Under Contract NAS3-25266

National Aeronautics and
Space Administration

Review of Nondiffracting Bessel Beams

Michael R. LaPointe
Sverdrup Technology, Inc.,
Lewis Research Center Group
Brook Park, Ohio

Abstract

The theory of nondiffracting Bessel beam propagation and experimental evidence for nearly-nondiffractive Bessel beam propagation are reviewed. The experimental results are reinterpreted using simple optics formulas, which show that the observed propagation distances are characteristic of the optical systems used to generate the beams and do not depend upon the initial beam profiles. A set of simple experiments are described which support this interpretation, and it is concluded that nondiffracting Bessel beam propagation has not yet been experimentally demonstrated.

I. Introduction

The distance over which a collimated, monochromatic beam will travel in free space without significant spreading is given by the Rayleigh distance[1]:

$$Z_R = \frac{\pi r_0^2}{\lambda} \tag{1}$$

where λ is the wavelength and r_0 is the initial radius of the beam. In 1983, Brittingham[2] discovered a new class of three-dimensional, packet-like solutions to Maxwell's free space wave equation, describing waves which propagate at the speed of light and remain focused for all time. These wave solutions had infinite energy, however, and required artificial discontinuities to produce real, nondispersive pulses with finite energy. Such discontinuities could not be propagated with a real antenna system, and the solutions remained theoretically interesting but physically unreal. A general procedure for obtaining packet-like solutions to the wave equation was subsequently published by Belanger[3], who showed that Brittingham's heuristically derived solutions could be generated using Gaussian Laguerre polynomials. The packet-like wave solutions found by Belanger also required infinite energy for nondiffractive propagation, however, and thus could not be produced in a real system.

In 1985, Ziolkowski[4] derived new, exact solutions to the free space wave equation in the form of nondispersive Gaussian pulses. Such waves could be launched with finite energy from a complex antenna, and Ziolkowski *et al.*[5] later performed experiments using acoustic waves in water to demonstrate apparently nondiffractive wave propagation. In 1987, Durnin[6] developed a nondiffracting zero-order Bessel function solution to the free space scalar wave equation. Soon thereafter, Durnin *et al.*[7] published experimental evidence for the nearly-nondiffractive nature of these waves, claiming propagation distances far exceeding the normal Rayleigh range before significant beam spreading was observed. Additional theoretical analyses describing nearly-nondiffracting electromagnetic missiles[8] and bullets[9] were published by various authors during this period, sparking a flurry of activity and a host of possible applications.

Nondiffracting beams have been suggested for use in remote power transmission[10,11], where such beams could significantly decrease transmitter and collector surface areas. The benefits for remotely powered spacecraft

propulsion and communication are obvious, and an effort was undertaken at the NASA Lewis Research Center to investigate the use of nondiffracting beams for spacecraft propulsion applications. Attention was focused on continuous-wave Bessel beams, which may be generated using fairly simple optical systems.

Section II outlines the nondiffracting, zero-order Bessel function solution to the free space wave equation, followed by a review of published Bessel beam propagation experiments in Section III. The experimental results are discussed and reinterpreted in Section IV, with concluding remarks presented in Section V.

II. Bessel Beam Theory

As shown by Durnin[6], the free space wave equation

$$\left(\nabla^2 - \frac{1}{c^2}\frac{\partial^2}{\partial t^2}\right)\psi(\vec{r},t) = 0 \tag{2}$$

has the exact solution:

$$\psi(x,y,z\geq 0,t) = \exp[i(k_z z - \omega t)]\int_0^{2\pi} A(\phi)\exp\left[ik_\perp\left(x\cos\phi + y\sin\phi\right)\right]d\phi \tag{3}$$

for a scalar field ψ propagating with velocity c into a source-free region $z \geq 0$. The wavelength λ and wave frequency ω are related to the magnitudes of the wave vectors parallel (k_z) and perpendicular ($k_\perp$) to the direction of propagation via:

$$\begin{aligned} \lambda &= 2\pi/\left(k_z^2 + k_\perp^2\right)^{1/2} \\ \omega &= c\left(k_z^2 + k_\perp^2\right)^{1/2} \end{aligned} \tag{4}$$

The axial z dependence is thus separated from the transverse x, y coordinates. When k_z is real, the solution represents a nondiffracting field in the sense that the time-averaged intensity I is independent of z:

$$\begin{aligned} I(x,y,z\geq 0) &= \frac{1}{2}\left|\psi(\vec{r},t)\right|^2 \\ &= I(x,y,z=0) \end{aligned} \tag{5}$$

The variable $A(\phi)$ in Equation 3 represents an arbitrary complex function of the angular coordinate ϕ. For solutions with complete axial symmetry, $A(\phi) \equiv 1$, and the nondiffracting scalar field solution may be written:

$$\begin{aligned} \psi(\vec{r},t) &= \exp[i(k_z z - \omega t)]\int_0^{2\pi}\exp\left[ik_\perp\left(x\cos\phi + y\sin\phi\right)\right]\frac{d\phi}{2\pi} \\ &= \exp[i(k_z z - \omega t)]J_0(k_\perp\rho) \end{aligned} \tag{6}$$

where J_0 is the zero-order Bessel function of the first kind and ρ is the radial position, defined:

$$\rho = \left(x^2 + y^2\right)^{1/2} \tag{7}$$

When $k_\perp$=0, the solution reduces to a plane wave traveling in the $+z$ direction. For $0 \leq k_\perp \leq \omega/c$, the solution represents a nondiffracting beam whose intensity profile radially decreases with increasing $k_\perp\rho$, as shown in Figure 1.

The amount of energy contained in each lobe of the zero-order Bessel distribution is roughly equal to the amount of energy contained in the central peak[6,10], and it would require an infinite amount of energy to

create a nondiffracting J_0 Bessel beam over an infinite plane. Use of an aperture to restrict the radial extent of the beam eliminates the infinite energy concern, but introduces edge diffraction effects which cause the beam to spread. Durnin[6] used numerical simulations to evaluate the propagation distance of the central peak in a Bessel beam of finite radius, and found that the central spot propagates significantly further than a Gaussian beam of equal diameter (Figure 2). The maximum propagation range of an apertured, nearly-nondiffracting J_0 Bessel beam was determined to be[6]:

$$Z_{max} = R\left[(2\pi/k_\perp\lambda)^2 - 1\right]^{1/2} \tag{8}$$

where R is the radius of the aperture in which the Bessel beam is formed, and Z_{max} is the formation distance of a conical shadow zone, which marks the maximum range of the beam (Figure 3).

III. Bessel Beam Experiments

Lenticular Generation of Bessel Beams

The propagation of an apertured Bessel beam was experimentally demonstrated by Durnin *et al.*[7] using the optical system shown in Figure 4. A circular slit with mean diameter $d = 2.5$ mm and slit width $\Delta d = 10\mu$m was placed at the focal plane of a lens with radius $R = 3.5$ mm and focal length $f = 305$ mm. The slit was illuminated with collimated light of wavelength $\lambda = 633$ nm, producing a J_0 Bessel beam distribution with a central spot wavenumber $k_\perp = (2\pi/\lambda)\sin\theta$, where $\theta = \tan^{-1}(d/2f)$ is the diffraction angle. Approximating the central spot radius $r_0 \approx 1/k_\perp$, Equation (8) yields a maximum beam propagation distance of:

$$Z_{max} = \frac{2\pi r_0 R}{\lambda} \tag{9}$$

When the lens (aperture) radius exceeds the central spot radius ($R \gg r_0$), the propagation range will exceed the Rayleigh range predicted by Equation (1). Using the numerical values given above, the central spot radius is approximately 25 μm, yielding an estimated maximum range of 85 cm. This agrees well with the experimental data shown in Figure 5, which plots the intensity of the central peak as a function of propagation distance[7]. In contrast, the predicted Rayleigh range for a 25μm radius beam is only 3 mm, and it would appear that the Bessel beam propagates much further than standard diffraction theory would predict.

Holographic Generation of Bessel Beams

Based on the results of Durnin[6], Vasara *et al.*[11] used computer-generated holograms to create a series of apparently nondiffracting, arbitrary-order Bessel beams (Figure 6). The holographic pattern used to produce an on-axis J_0 Bessel beam is shown in Figure 7. The diffraction patterns are computer generated, printed with a high quality laser printer, and photoreduced onto photographic film (resolution = 5000 lines/m) to create the final hologram.

Upon illumination, the intensity distribution in the plane behind the hologram is given by:

$$I(x,y,z) \propto z\left|\int_0^{2\pi} A(\phi)\exp[-i2\pi k(x\cos\phi + y\sin\phi)/\gamma]d\phi\right|^2 \tag{10}$$

where k is the wavenumber ($2\pi/\lambda$), ρ_0 is the hologram fringe spacing ($2\pi/k_\perp$), and the parameter $\gamma \equiv \rho_0 k$, with the other symbols defined above. Using geometric optics (Figure 8), the maximum propagation distance was predicted to be:

$$Z_{max} = \frac{\gamma R}{2\pi} \tag{11}$$

where R defines the hologram (aperture) radius. Substituting for γ, k, and ρ_0, and assuming $r_0 = 1/k_\perp$ as before, yields:

$$\begin{aligned} Z_{max} = \frac{\gamma R}{2\pi} = \frac{\rho_0 k R}{2\pi} &= \frac{2\pi R}{k_\perp \lambda} \\ &= \frac{2\pi r_0 R}{\lambda} \end{aligned} \tag{12}$$

in agreement with the maximum propagation distance predicted by Equation 9.

The holograms were illuminated with laser light at $\lambda = 633$ nm, yielding axial intensity distributions similar to the distribution shown in Figure 9. For a hologram with $\rho_0 = 1$ mm (r_0=1.59×10^{-4} m) and $R = 10$ mm, the maximum propagation distance of a J_0 Bessel beam was found to be 15.8 m; for a hologram with $\rho_0 =$ 1 mm and $R = 8$ mm, the maximum propagation distance was 12.6 m. Both values are substantially larger than the Rayleigh propagation distance of 12.5 cm expected for a well collimated beam with an initial radius of 1.59×10^{-4} m.

IV. Discussion

The experiments outlined above appear to substantiate the nearly-nondiffractive nature of the Bessel beam distributions. However, alternative explanations of the experimental results are presented below which question the nondiffracting wave interpretation.

Equivalent Beam Comparisons

Both experiments[7,11] report extended propagation distances for the Bessel beam central spot when compared to the expected Rayleigh distances for Gaussian beams of equal diameter (*cf* Figure 2). However, the full Bessel beam consists of not only the central peak but the full complement of ancillary lobes in the Bessel distribution (Figures 1, 6). The Bessel beam propagation should thus be compared to a Gaussian beam whose radius equals the full Bessel beam radius, not the radius of the central peak alone. The radius of the full Bessel beam propagated by Durnin *et al.*[7] was 3.5 mm, set by the optical system aperture lens. From Equation 1, the expected Rayleigh distance for a well collimated, 3.5 mm radius beam with a wavelength of 633 nm is approximately 61 meters, significantly farther than the 85 cm beam propagation distance reported by Durnin *et al.* Similar arguments hold for the holographically generated Bessel distributions, where the full hologram diameters should be used for the beam comparisons. A well collimated beam with a wavelength of 633 nm and a radius equal to the hologram radius of 10 mm will propagate almost 500 m without spreading, a significantly longer distance than the reported Bessel beam propagation length of 15.8 meters. The central peaks in the Bessel beam distributions do persist over distances longer than expected for collimated beams with diameters equal to the central spot diameters; however, the central peaks cannot be produced without the full Bessel beam distribution. When compared to the propagation distances of beams with fully equal diameters, the reported Bessel beam propagation distances do not appear to justify claims of nearly-nondiffracting wave propagation.

Similar concerns with the reported beam comparisons have recently been published by Sprangle and Hafizi[12]. For a Bessel beam with N lobes, they suggest that the appropriate beam diameter to use for comparison is $R = Nr_0$, where r_0 is the central spot radius. The correct propagation distance for the Bessel beam central spot is then given by:

$$Z_{max} = \frac{R}{\tan\theta} = \frac{2Rr_0}{\lambda} = \frac{2Nr_0^2}{\lambda} \tag{13}$$

where $\tan\theta \approx \theta \approx k_\perp/k_z \approx \lambda/2r_0$ is the diffraction angle of the beam. For comparison, the Rayleigh propagation distance for a well collimated beam with radius R is given by Equation 1:

$$Z_R = \frac{\pi R^2}{\lambda} = \frac{\pi R(Nr_0)}{\lambda} \tag{14}$$

Equating the propagation distances given by Equations 13 and 14 yields:

$$Z_{max} = \frac{2}{\pi N} Z_R \tag{15}$$

which shows that any well collimated beam of radius R will travel $\pi N/2$ times further than the Bessel beam, in qualitative agreement with the previous discussion.

In rebuttal to Sprangle and Hafizi, Durnin *et al.*[13] repeat their claim that the central peak intensity is "remarkably resistant to the diffractive spreading commonly associated with all wave propagation", and offer as further proof the beam profiles displayed in Figures 10a and 10b. Figure 10a shows the beam distribution after propagating a distance of 15 cm, and Figure 10b shows the beam profile, essentially unchanged, after propagating a distance of 100 cm. The central peak has a diameter of approximately 70 μm, and were that the full extent of the Bessel beam, it would indeed be a remarkable propagation measurement. However, the radius of the full Bessel beam, as noted in the figures, is 0.5 mm, and the expected Rayleigh distance for a well collimated, 633 nm wavelength, 0.5 mm radius beam is 124 cm; it is therefore not surprising that the beam has not diverged at 100 cm. The reported propagation distance is consistent with the propagation of any well collimated beam with similar dimensions, and does not constitute proof of nearly-nondiffracting beam propagation.

Optical System Characteristics

Additional arguments based on geometric optics can be used to show that the reported propagation distances are actually characteristic of the systems used to generate the beams, rather than intrinsic properties associated with the Bessel beam profiles.

Apertured Lens System

The optical system used by Durnin *et al*[7] to create Bessel beam distributions is redrawn in Figure 11, which illustrates the elementary, single lens nature of the optical system. The system may be analyzed using the simple thin-lens formula[14]:

$$\frac{1}{s_o} + \frac{1}{s_i} = \frac{1}{f} \tag{16}$$

where s_o is the object distance, s_i is the image distance, and f is the focal length of the lens. Rearranging the lens formula yields:

$$s_i = \frac{s_o f}{s_o - f} \tag{17}$$

for the image distance, which is equivalent to the maximum propagation distance before the beam starts to expand. From Figure 11, the diffraction angle θ for the beam leaving the circular slit is given by

$$\tan\theta \approx \theta \approx \frac{D}{f+\delta} \tag{18}$$

where D is the beam diameter at the aperture lens and $f+\delta$ is the equivalent object distance for the system. From the same figure, the distance δ is related to the diffraction angle θ and the circular slit diameter d via:

$$\tan\theta \approx \theta \approx \frac{d}{\delta} \tag{19}$$

which yields the relation:

$$\theta \approx \frac{d}{\delta} = \frac{D}{f+\delta} \tag{20}$$

or

$$\frac{f+\delta}{\delta} = \frac{D}{d} \tag{21}$$

Substituting Z_{max} for the image distance and $f+\delta$ for the object distance in Equation 17 yields:

$$Z_{max} = \frac{s_o f}{s_o - f} = \frac{(f+\delta)f}{(f+\delta)-f} = \frac{f(f+\delta)}{\delta} \tag{22}$$

which, with the use of Equation 21, reduces to

$$Z_{max} = \frac{fD}{d} \tag{23}$$

for the maximum propagation distance expected in the optical system. Substituting the values used by Durnin *et al.*[7] for f, D, and d (305 mm, 7 mm, and 2.5 mm, respectively) yields a maximum propagation distance of 85 cm, in exact agreement with the experimentally measured value. It is important to note that no assumption was made concerning the initial beam profile in the derivation of Equation 23. The circular slit could be replaced with an iris diaphragm of equivalent diameter, and the resulting beam would propagate exactly the same distance as the Bessel beam created with the annular slit. The propagation distance is characteristic of the optical system, as specified by the initial beam diameter d at the focal plane of the lens, the expanded beam diameter D at the lens, and the focal length f of the lens.

A set of simple experiments were performed to verify that the propagation distances were intrinsic to the optical system and not the initial beam distribution. A low power, 633 nm laser beam was expanded, collimated, and sent through an adjustable iris aperture (Figure 12). A window fitted with a central 1 mm diameter opaque disk was placed adjacent to the iris aperture, and the iris was closed until a circular slit geometry was approximated (Figure 13a). The expanded beam passed through the iris/window combination, producing a zero-order Bessel function intensity distribution in the beam. The beam was recollimated and sent to a set of sizing lenses, whose purpose was to adjust the beam size and provide flexibility in the optical system parameters (Figure 13b). The second beam collimation was required to provide accurate measurements of the object and image distances used to adjust the sizing lens array. The first sizing lens produces a focused image of the circular slit and Bessel beam intensity distribution; this real image then acts as a real object for the second (aperture) lens. This part of the system is equivalent to the optical system used by Durnin *et al.*[7], with the material circular slit replaced by a real image of the circular slit and the second sizing lens assuming the role of the aperture lens (compare Figures 4 and 13b).

For the beam propagation experiments reported below, the focal length of the first sizing lens was 5.19 cm, the focal length of the second (aperture) lens was 10.2 cm, and the lenses were separated a distance of 16.5

cm. Using Figure 13b, the value of δ is thus 1.1 cm, and the expected propagation distance from Equation 22 is approximately 105 cm. This propagation distance is characteristic of the optical system, and does not depend upon the intensity profile of the beam propagating through the system.

Figure 14 plots the central peak intensity versus propagation distance for the Bessel beam distribution generated with the iris/window combination described above. The central spot intensity reaches a maximum value at a distance approximately 110 cm away from the aperture lens, in good agreement with the propagation distance estimated above. Slight misalignments in the beam collimation will cause small errors in the location of the circular slit image, which accounts for the slight discrepancy in the predicted and measured maximum propagation distances. The intensity profile across the beam was measured with a 1024 element diode array. Beam profiles at 54 cm, 110 cm, 130 cm, and 250 cm away from the aperture lens are displayed in Figures 15a through 15d. The central peak is clearly visible in Figure 15a, with the surrounding lobe intensity decreasing radially away from the central peak. The distribution has been radially compressed in Figure 15b due to focusing by the optical system, with the peak intensity reaching almost 9 times the peak intensity recorded at 54 cm. The distribution then splits into a doubled peak distribution (Figure 15c), reflecting the edge focusing effects of the lens system. As the beam propagates further, the Bessel distribution reappears at a much reduced intensity (Figure 15d). The beam profile retains this Bessel distribution, with decreasing intensity, for the remainder of the measured propagation distance.

A second beam profile was then introduced into the system using a 10 μm pinhole in place of the iris/window combination. The intensity distribution at a distance 54 cm from the aperture lens is displayed in Figure 16a, and shows a flat central beam region with intensity spikes at the beam periphery, which again correspond to edge focusing effects. The beam profiles at 105 cm and 124 cm are shown in Figures 16b and 16c, respectively, and the on-axis central beam intensity versus propagation distance is displayed in Figure 17. The maximum intensity occurs at approximately 105 cm, again in agreement with the maximum propagation distance expected for the optical system. Both the Bessel beam distribution and the flat central beam distribution have the same maximum propagation distances, within experimental error, indicating that the propagation distances are characteristic of the system and do not depend on the initial beam intensity profiles.

Holographic Lens System

The propagation of Bessel beams generated holographically can also be explained in terms of the holographic system used to produce the beams, rather than propagation properties intrinsic to the Bessel beam distribution. As discussed by Hecht[15], a hologram may be described as a superposition of simple Fresnel zone plates (Figure 18). A zone plate acts like a crude lens, diffracting collimated light into a beam which converges to a real focal point. The similarity between the hologram creating the J_0 Bessel beam (Figure 7) and a simple Fresnel zone plate (Figure 18) is apparent.

The primary focal length of a zone plate is given by[16]:

$$f = \frac{R_m^2}{m\lambda} \tag{24}$$

where m is the number of zones (rings) in a zone plate of radius R_m, and λ is the wavelength of light diffracted by the zone plate. The holograms used by Vasara *et al.*[11] had radii of 8 mm and 10 mm, with 1 mm spaces between the rings in each of the holograms. The number of rings m in each hologram were thus 8 and 10, respectively. The holograms were illuminated with collimated laser light at 633 nm. Substituting these values into Equation 24 yields a focal length of 12.6 m for the 8 mm radius hologram and 15.8 m for the 10 mm hologram, in exact agreement with the experimentally reported propagation distances. Again, no assumptions were made concerning Bessel beam properties; the propagation distances are a result of the zone plate nature of the holograms used to generate the beam distributions. Similar results would be obtained with other beam distributions; the maximum propagation distances would correspond to the focal

plane of the equivalent zone plates.

V. Conclusions

Bessel function solutions to the free space wave equation require infinite energy for nondiffractive propagation. Finite energy approximations to the nondiffracting Bessel function solutions may be realized by generating the Bessel distribution within an aperture; however, the aperture introduces diffraction in the beam, causing the beam to spread with distance. Nearly-nondiffractive Bessel beam propagation has been reported by authors using aperture lenses and holographic techniques to generate finite-radius Bessel beam distributions. Propagation distances for the central peak of the Bessel distribution exceed the Rayleigh distance for the propagation of well collimated beams with radii equal to the central spot radius. However, it is shown that a proper comparison of propagation distances requires the full Bessel distribution radius to be used, and the reported propagation distances are actually much shorter than the standard Rayleigh distances calculated for beams of full equivalent radius. It is further shown that the reported propagation distances are a result of the optical systems used to generate the beams, and do not depend upon the initial beam intensity profiles. A set of simple experiments were performed to verify the analysis, and it is concluded that nondiffracting Bessel beam propagation has not yet been experimentally demonstrated.

References

1. Siegman, A. E., *An Introduction to Lasers and Masers*, McGraw-Hill Book Co., New York, New York, 1971, pp.313-314.

2. Brittingham, J. N., "Focus Wave Modes in Homogeneous Maxwell's Equations: Transverse Electric Mode", *J. Appl. Phys.*, **54** (3), March 1983, pp. 1179-1189.

3. Belanger, P. A., "Packetlike Solutions of the Homogeneous-Wave Equation"', *J. Opt. Soc. Am. A*, **1** (7), July 1984, pp. 723-724.

4. Ziolkowski, R. W., "Exact Solutions of the Wave Equation with Complex Source Locations", *J. Math. Phys.*, **26** (4), April 1985, pp. 861-863.

5. Ziolkowski, R. W., Lewis, D. K., and Cook, B. D., "Evidence of Localized Wave Transmission", *Phys. Rev. Let.*, **62** (2), January 1989, pp. 147-150.

6. Durnin, J., "Exact Solutions for Nondiffracting Beams. I: The Scalar Theory", *J. Opt. Soc. Am. A*, **4** (4), April 1987, pp. 651-654.

7. Durnin, J., Miceli, J. J. Jr., and Eberly, J. H., "Diffraction-Free Beams", *Phys. Rev. Let.*, **58** (15), April 1987, pp. 1499-1501.

8. Shen, H. and Wu, T., "The Transverse Energy Pattern of an Electromagnetic Missile from a Circular Current Disk", *Microwave and Particle Beam Sources and Directed Energy Concepts*, **SPIE 1061**, 1989, pp. 352-360.

9. Moses, H. E. and Prosser, R. T., "Acoustic and Electromagnetic Bullets", *Microwave and Particle Beam Sources and Directed Energy Concepts*, **SPIE 1061**, 1989, pp. 403-416.

10. Durnin, J., Miceli, J. J. Jr., and Eberly, J. H., "Comparison of Bessel and Gaussian Beams", *Optics Letters*, **13** (2), February 1988, pp. 79-80.

11. Vasara, A., Turunen, J., and Friberg, A. T., "Realization of General Nondiffracting Beams with Computer-Generated Holograms", *J. Opt. Soc. Am. A*, **6** (11), November 1989, pp. 1748-1754.

12. Sprangle, P. and Hafizi, B., "Comment on Nondiffracting Beams", *Phys. Rev. Let.*, **66** (6), February 1991, p. 837.

13. Durnin, J., Miceli, J. J. Jr., and Eberly, J. H., "Reply to 'Comment on Nondiffracting Beams' ", *Phys. Rev. Let.*, **66** (6), February 1991, p.838.

14. Hecht, E., *Optics*, second edition, Addison-Wesley Pub. Co., Reading, MA, 1987, p. 137.

15. *ibid.*, p. 595.

16. *ibid.*, p. 446.

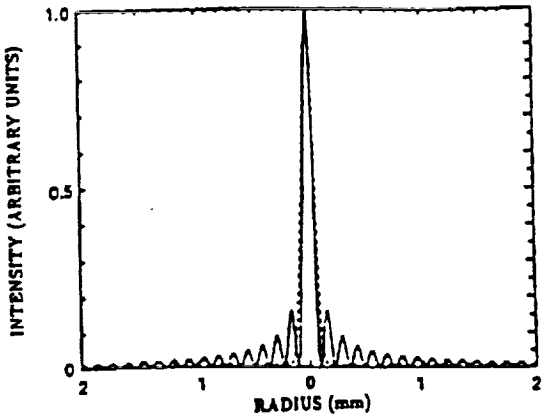

Figure 1. "Nondiffracting" Bessel beam intensity distribution. Adapted from Ref. 6.

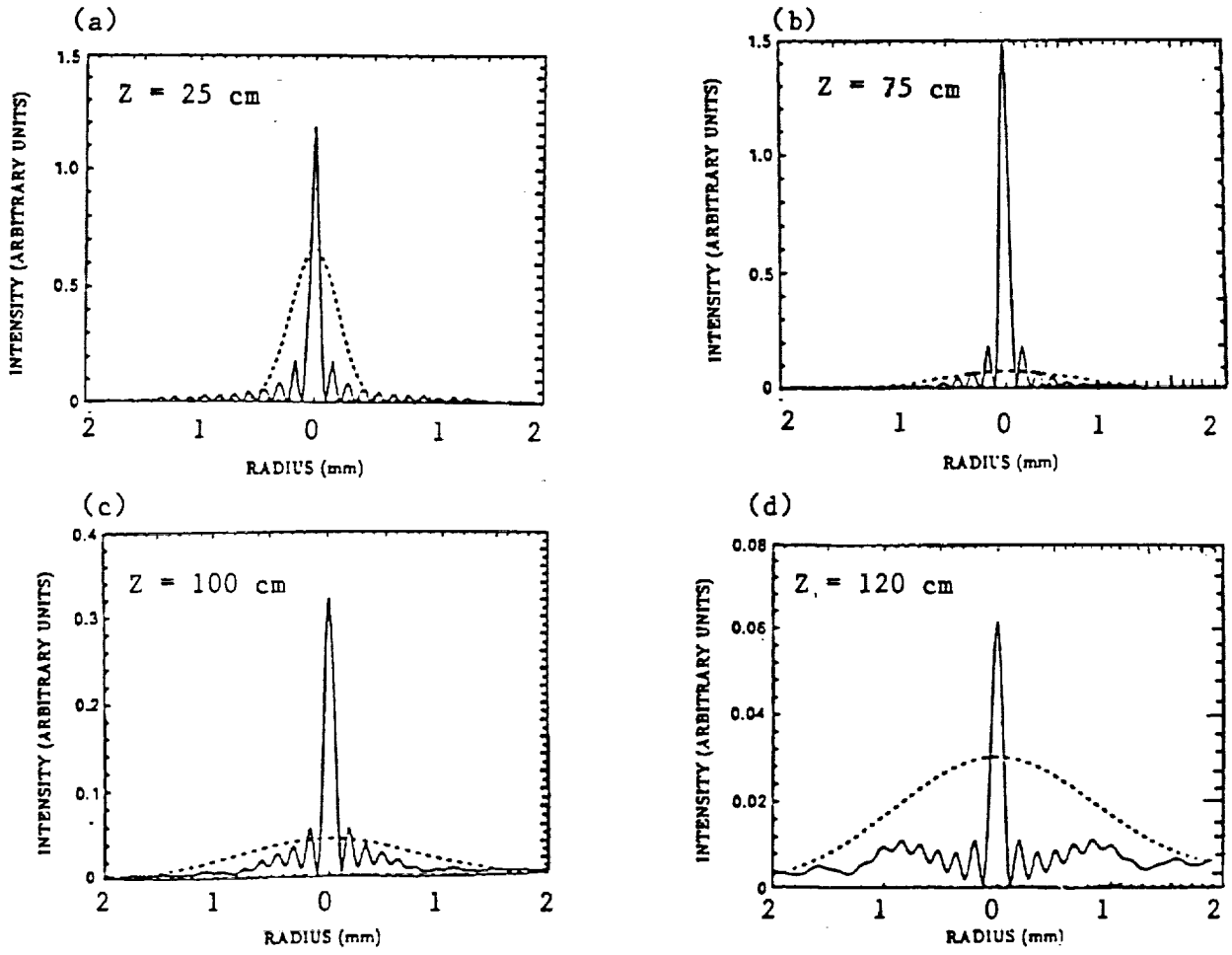

Figure 2. Calculated Bessel beam (solid) and Gaussian beam (dashed) intensity distributions for propagation distances of (a) 25 cm, (b) 75 cm, (c) 100 cm, and (d) 120 cm. Initial Gaussian beam diameter is assumed equal to Bessel beam central peak diameter, as shown in Figure 1. Assumed wavelength = 0.5 μm, arbitrary intensity units. Adapted from Ref. 6.

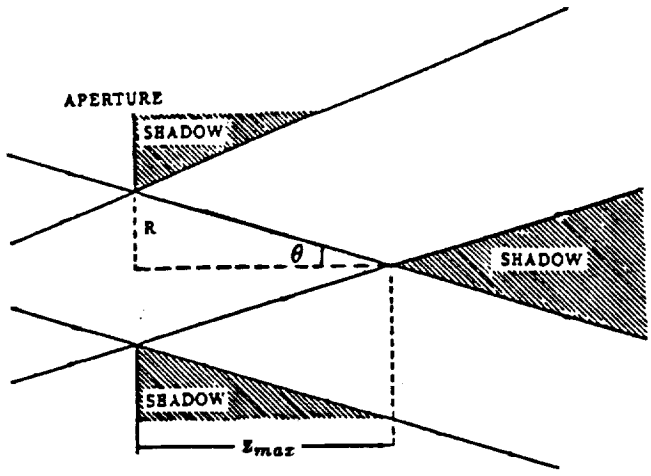

Figure 3. Geometric optics construction of J_0 Bessel beam propagation. Start of shadow zone marks maximum beam propagation distance. Adapted from Ref. 6.

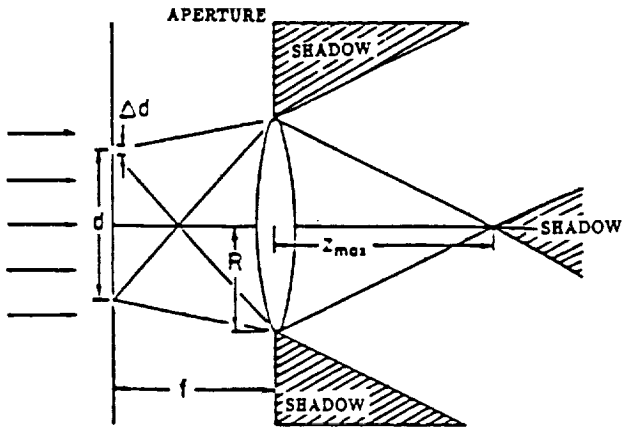

Figure 4. Arrangement used by Durnin *et al.*[7] for Bessel beam propagation experiments. (Not to scale)

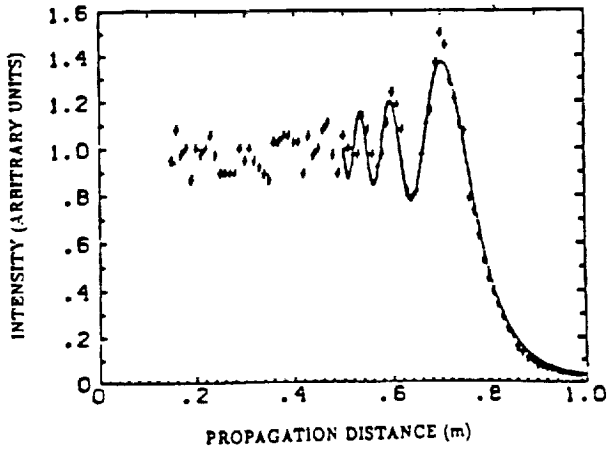

Figure 5. Measured (+) and calculated (solid) on-axis Bessel beam central peak intensity (arbitrary units). Adapted from Ref. 7.

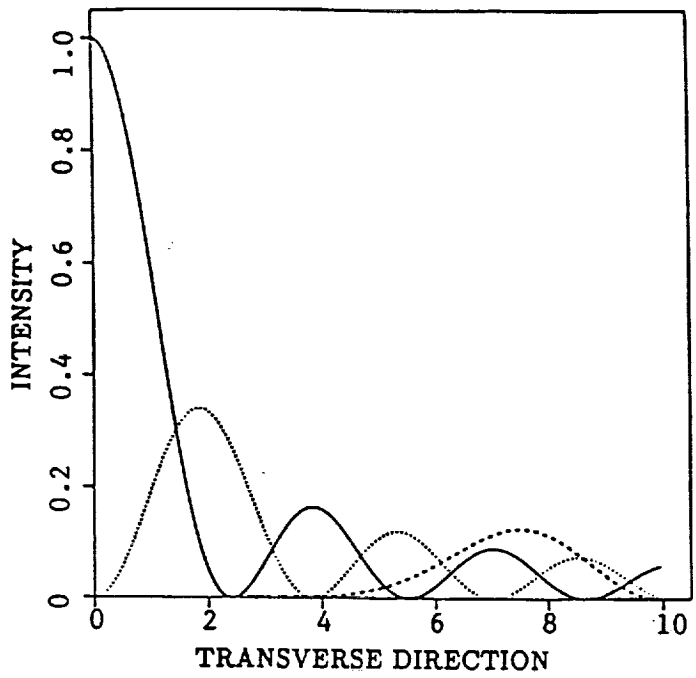

Figure 6. Radial intensity distributions corresponding to J_0, J_1, and J_6 Bessel beams. Adapted from Ref. 11.

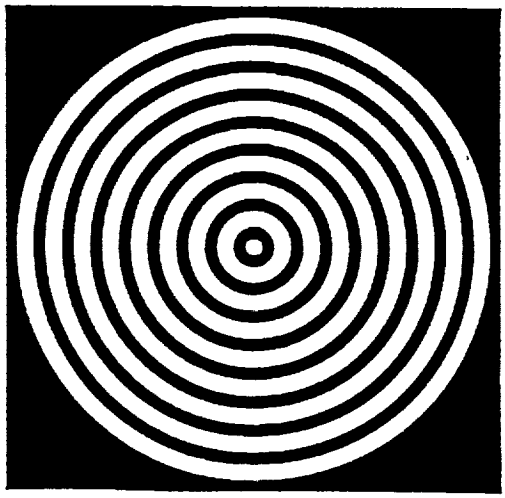

Figure 7. On-axis hologram used to generate J_0 Bessel beam distribution. Adapted from Ref. 11.

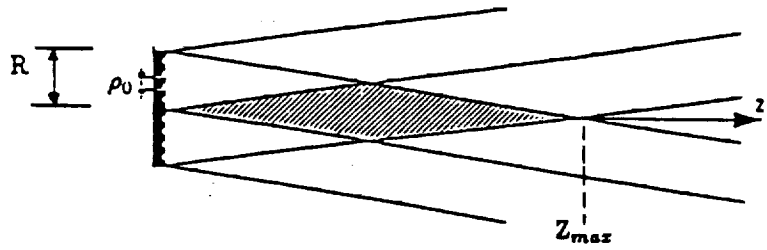

Figure 8. Geometric optics construction for holographically produced J_0 Bessel beam. Adapted from Ref. 11.

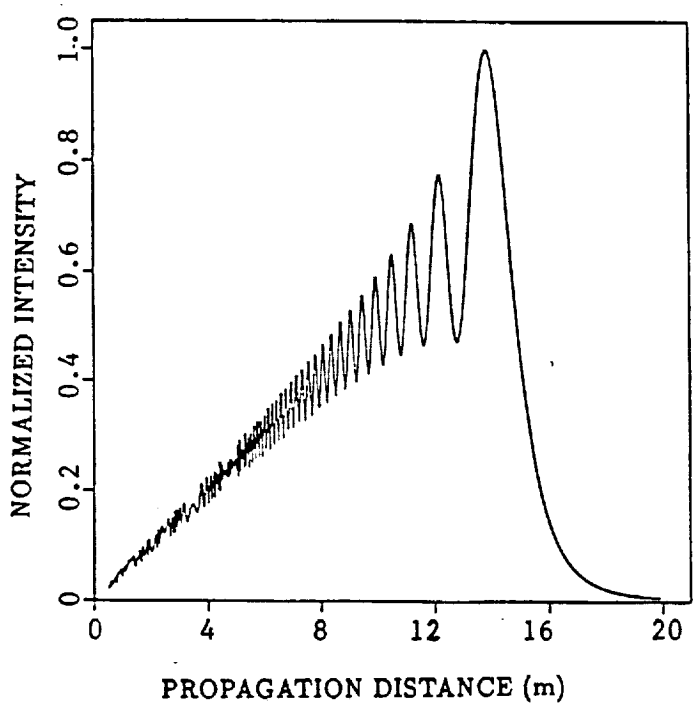

Figure 9. Typical on-axis J_0 Bessel beam intensity distribution versus propagation distance. Hologram radius = 2 cm, fringe separation 0.5 mm. Arbitrary intensity units. Adapted from Ref. 11.

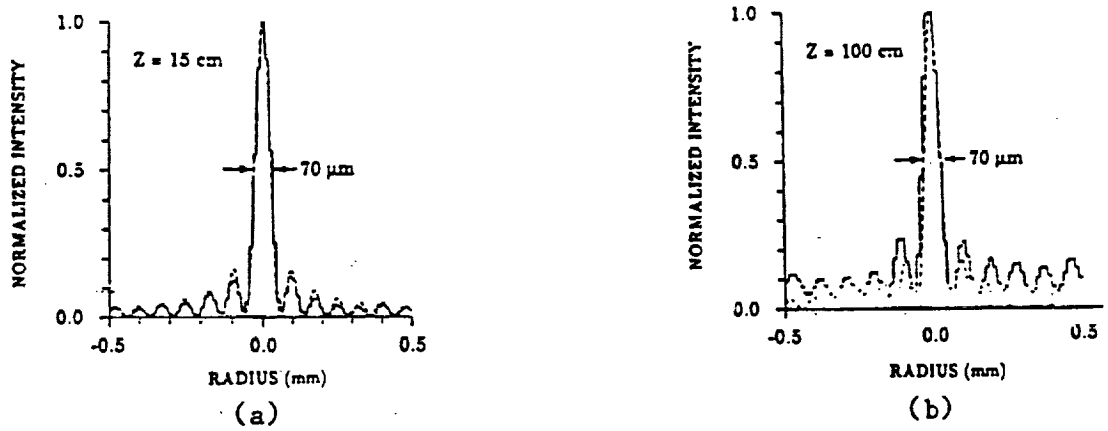

Figure 10. On-axis J_0 Bessel beam intensity distribution measured at (a) 15 cm and (b) 100 cm from aperture lens. Adapted from Ref. 13.

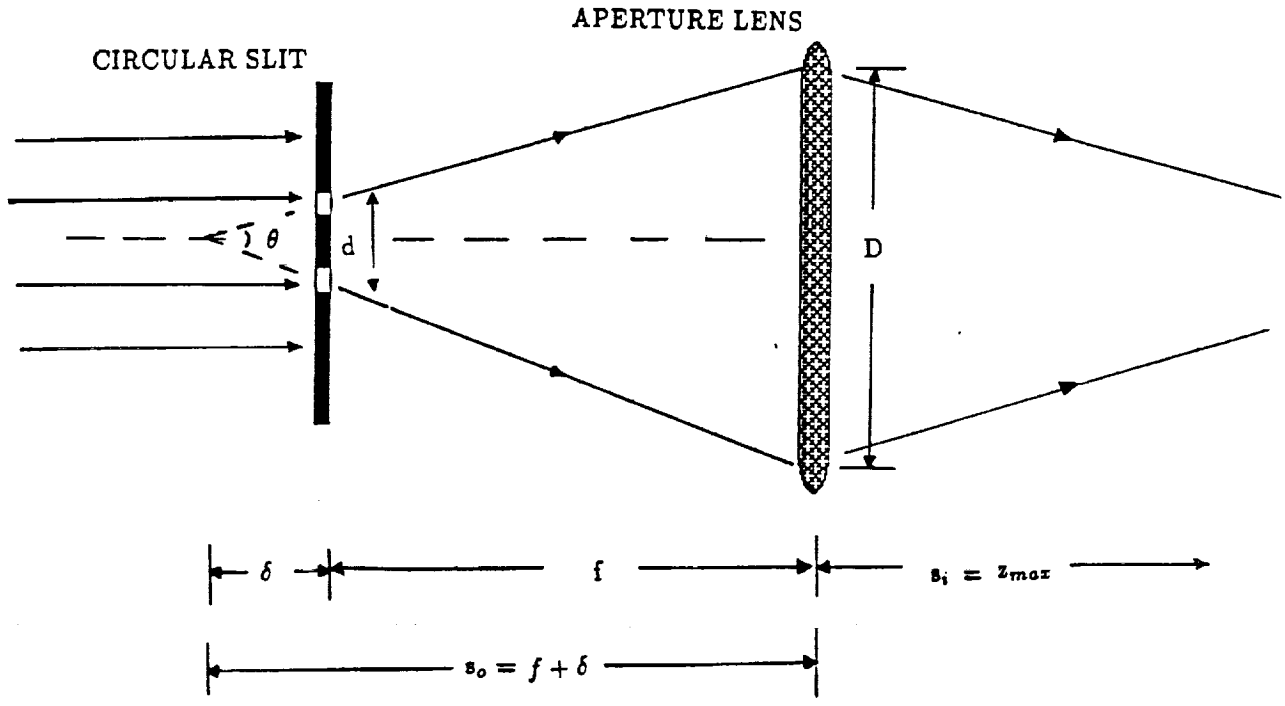

Figure 11. Geometric construction of Bessel beam experiment shown in Figure 4.

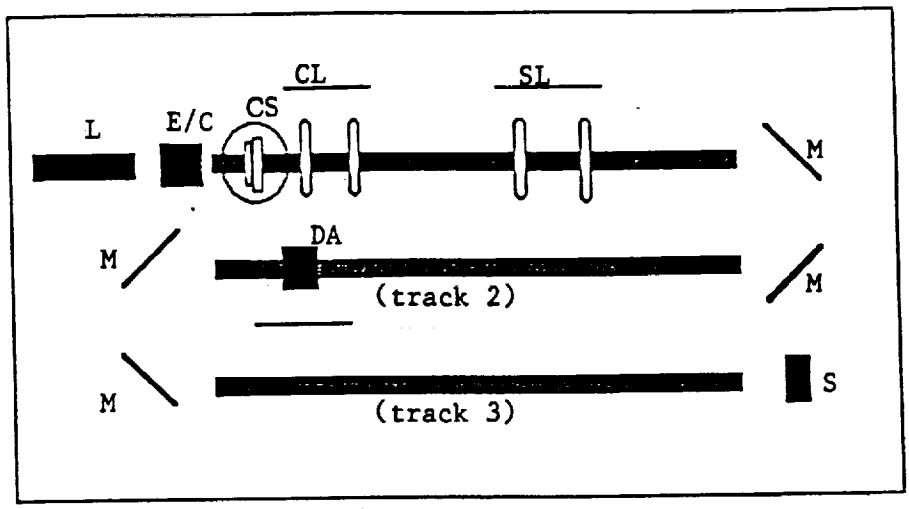

Figure 12. Optical table layout for producing Bessel beam distributions. Laser light (L) is expanded and collimated (E/C) and sent through the circular slit arrangement (CS) diagrammed in Figure 13. The beam is recollimated (CL) and sent to a set of sizing lenses (SL). The first sizing lens produces a real image of the circular slit/Bessel beam distribution, which acts as a real object for the second (aperture) lens. The beam is bounced off a set of mirrors (M) and directed along an optical path toward the diode array detector (DA). Additional mirrors provide access to a second optical path if desired. The beam terminates in the array detector or a beam stop (S).

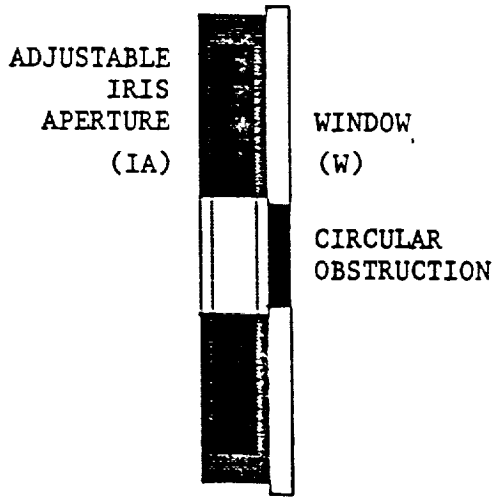

Figure 13(a). Schematic of circular slit arrangement used in Figure 12. An adjustable iris aperture (IA) is fitted with a window (W) on which is placed a central circular opaque obstruction. The iris is closed until a thin circular slit is approximated. The construction allows a variety of circular slit widths to be approximated.

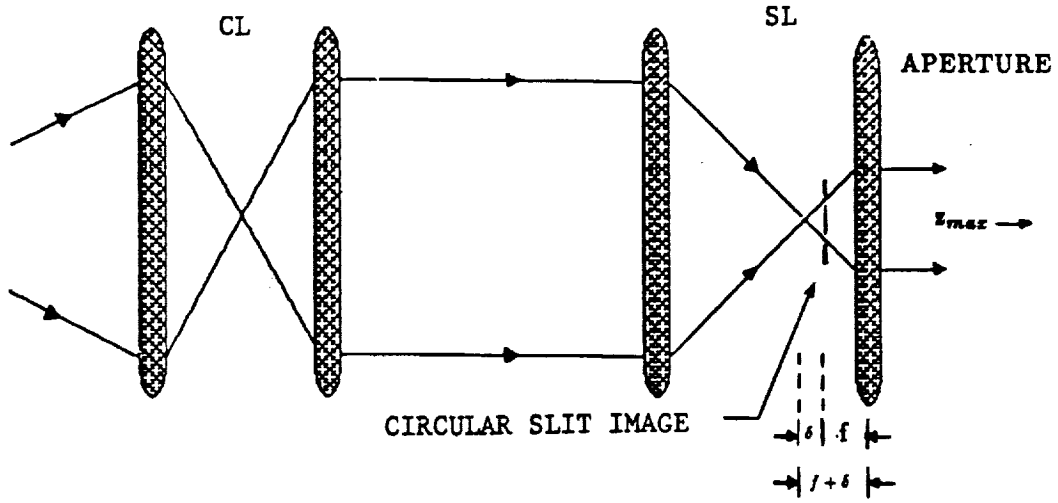

Figure 13(b). Schematic of collimating lens set (CL) and sizing lens set (SL) used in Figure 12. The first sizing lens creates a real image of the circular slit (Fig 13a) and Bessel beam distribution, which is then used as a real object by the second (aperture) lens. The collimating lenses allow accurate measurement of the image locations.

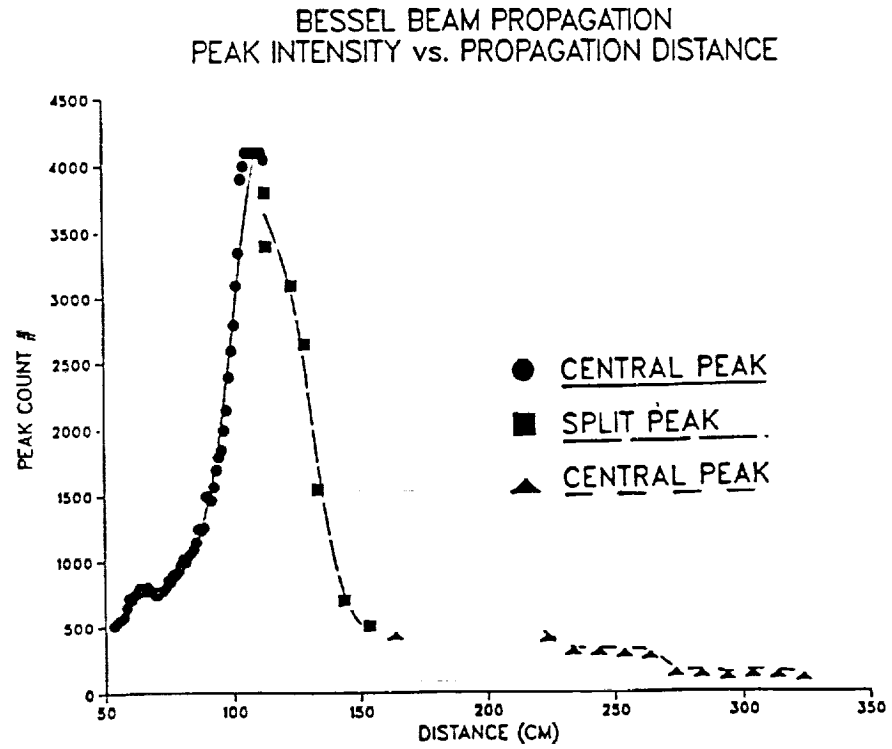

Figure 14. Measured intensity of on-axis Bessel beam central peak intensity (arbitrary units) vs. propagation distance. The beam starts as a Bessel distribution with a well defined central peak (circles), evolves to a binary peak distribution due to lens focusing effects (squares), and returns to a Bessel distribution further along the path (triangles); see Figure 16. Missing data correspond to the mirror paths between track 2 and track 3, shown in Figure 12.

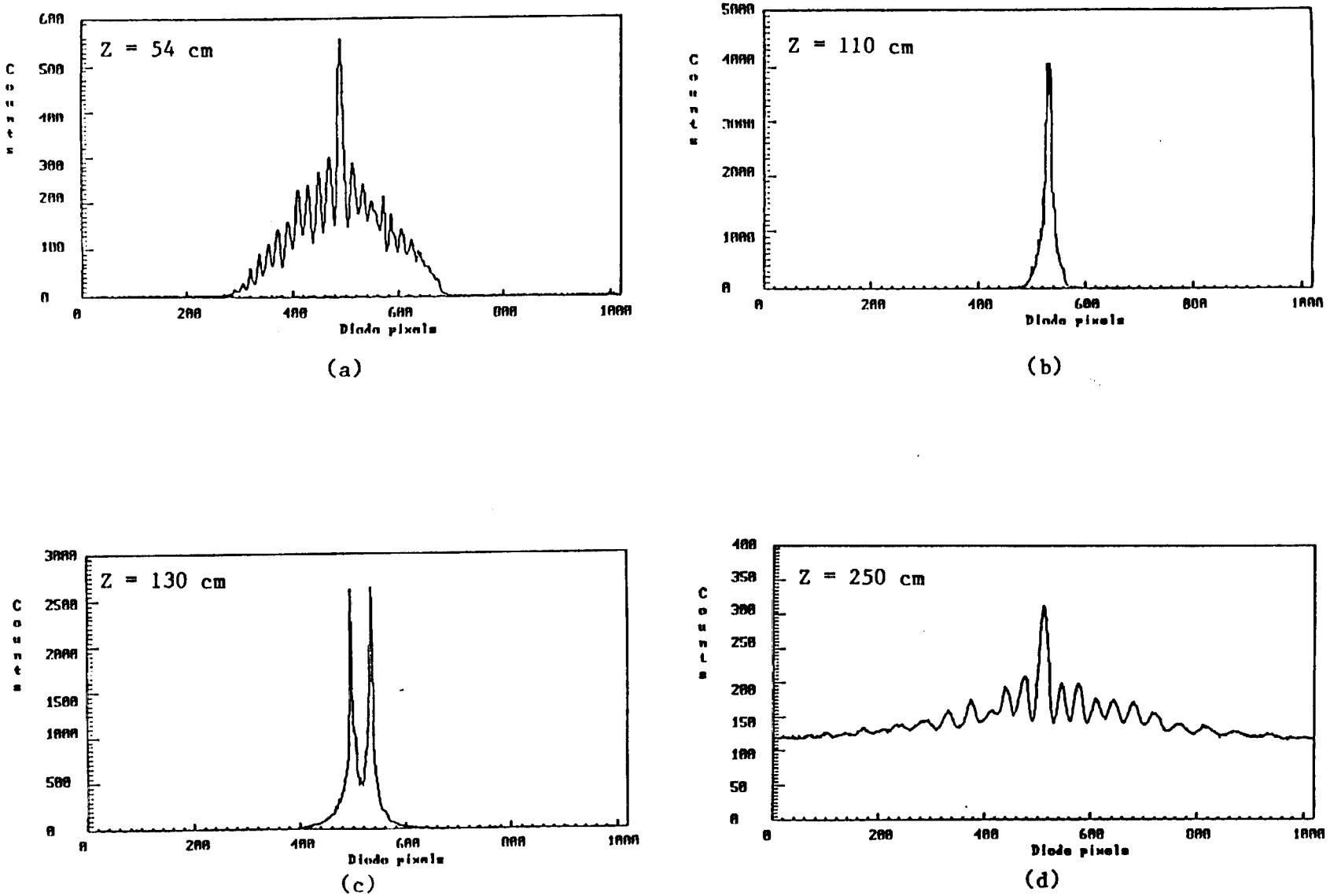

Figure 15. Bessel beam intensity distribution measurements at (a) 54 cm, (b) 110 cm, (c) 130 cm, and (d) 250 cm from aperture lens

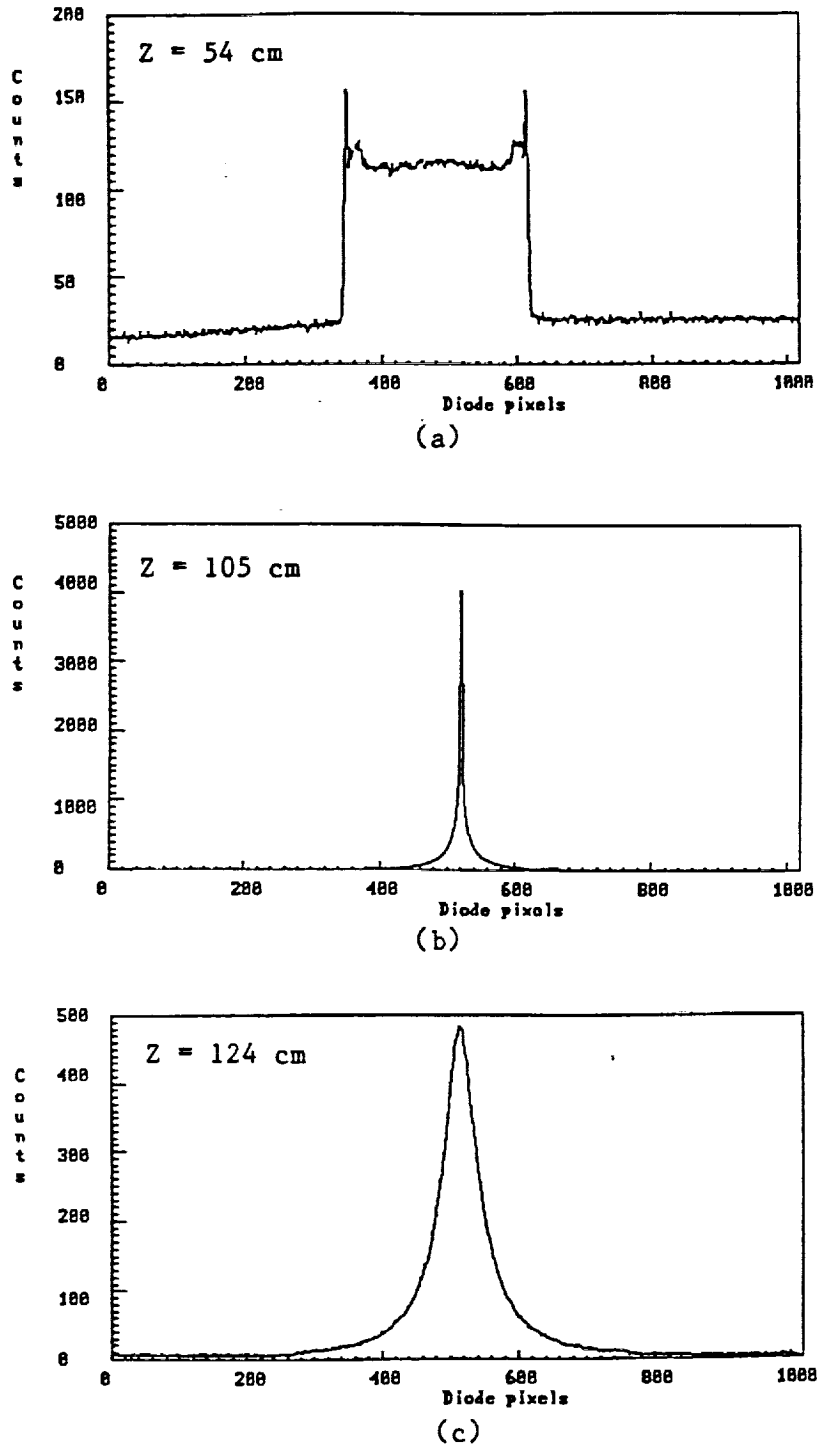

Figure 16. Clipped planar beam intensity profiles at (a) 54 cm, (b) 105 cm, and (c) 124 cm from aperture lens.

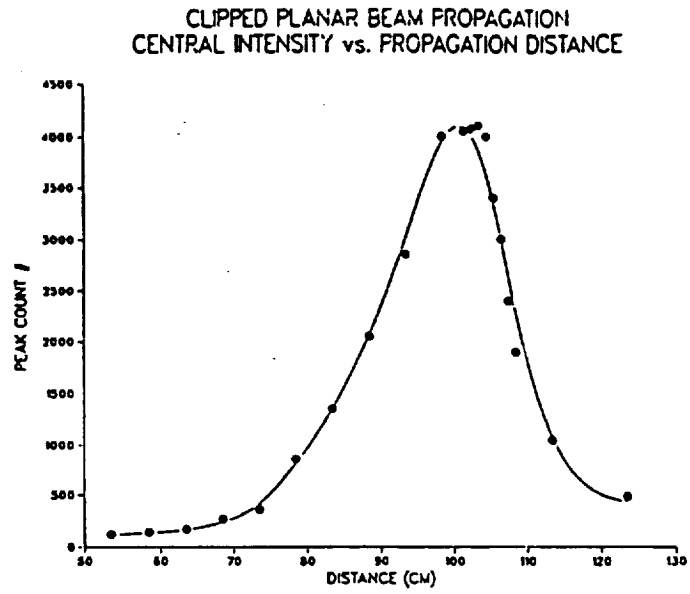

Figure 17. Measured intensity of clipped planar beam central intensity (arbitrary units) vs. propagation distance.

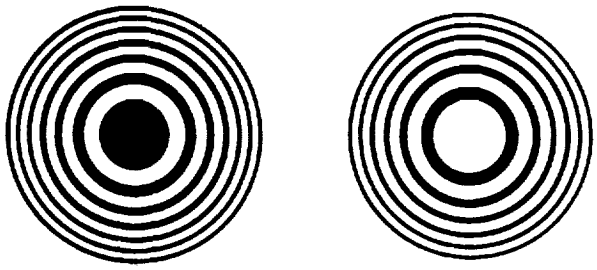

Figure 18. Fresnel zone plates.

REPORT DOCUMENTATION PAGE

Form Approved
OMB No. 0704-0188

1. AGENCY USE ONLY (*Leave blank*)	2. REPORT DATE	3. REPORT TYPE AND DATES COVERED
	August 1991	Final Contractor Report

4. TITLE AND SUBTITLE
Review of Nondiffracting Bessel Beams

5. FUNDING NUMBERS
WU-506-42-31
C-NAS3-25266

6. AUTHOR(S)
Michael R. LaPointe

7. PERFORMING ORGANIZATION NAME(S) AND ADDRESS(ES)
Sverdrup Technology, Inc.
Lewis Research Center Group
2001 Aerospace Parkway
Brook Park, Ohio 44142

8. PERFORMING ORGANIZATION REPORT NUMBER
E-6480

9. SPONSORING/MONITORING AGENCY NAMES(S) AND ADDRESS(ES)
National Aeronautics and Space Administration
Lewis Research Center
Cleveland, Ohio 44135-3191

10. SPONSORING/MONITORING AGENCY REPORT NUMBER
NASA CR-187188

11. SUPPLEMENTARY NOTES
Project Manager, James S. Sovey, Space Propulsion Technology Division, NASA Lewis Research Center, (216) 433-2420. Prepared for the 36th Annual International Symposium on Optical and Optoelectronic Applied Science and Engineering sponsored by the Society of Photo-Optical Instrumentation Engineers, San Diego, California, July 21-26, 1991.

12a. DISTRIBUTION/AVAILABILITY STATEMENT
Unclassified - Unlimited
Subject Category 74

12b. DISTRIBUTION CODE

13. ABSTRACT (*Maximum 200 words*)

The theory of nondiffracting Bessel beam propagation and experimental evidence of nearly-nondiffractive Bessel beam propagation are reviewed. The experimental results are reinterpreted using simple optics formulas, which show that the observed propagation distances are characteristic of the optical systems used to generate the beams and do not depend upon the initial beam profiles. A set of simple experiments are described which support this interpretation, and it is concluded that nondiffracting Bessel beam propagation has not yet been experimentally demonstrated.

14. SUBJECT TERMS	15. NUMBER OF PAGES
Diffraction; Optics; Light beams	20
	16. PRICE CODE: A03

17. SECURITY CLASSIFICATION OF REPORT	18. SECURITY CLASSIFICATION OF THIS PAGE	19. SECURITY CLASSIFICATION OF ABSTRACT	20. LIMITATION OF ABSTRACT
Unclassified	Unclassified	Unclassified	